Asian Journal of Chemistry; Vol. 37, No. 9 (2025), 2141-2154
ASIAN JOURNAL OF CHEMISTRY
https://doi.org/10.14233/ajchem.2025.34150

Pyrazole Containing Morpholine Moiety Compound: Bridging Experiment and Theoretical Investigation through Spectroscopy and Quantum Methods with Special Reference to NLO and Molecular Docking Insights

C. BAVANI[1], PERIYASAMY PRITHA[1], GOVINDARAJALU KISHORE[1], D. BHAKIARAJ[2], S. XAVIER[1,*] and S. SEBASTIAN[1]

[1]Department of Physics, St. Joseph's College of Arts & Science (Autonomous), Cuddalore-607001, India
[2]Department of Chemistry, St. Joseph's College of Arts & Science (Autonomous), Cuddalore-607001, India

*Corresponding author: E-mail: xavier@sjctnc.edu.in

Received: 29 May 2025 *Accepted*: 18 July 2025 *Published online*: 30 August 2025 AJC-22093

The current study carefully explores the spectroscopic and molecular structural studies of 4-(4,5-dihydro-3-(4-morpholinophenyl)-1*H*-pyrazol-5-yl)-*N*,*N*-dimethylbenzenamine (DMH). Theoretical calculations were computed at the B3LYP functional and 6-311G(d,p) basis set, which was compared with experimental UV-vis and FT-IR investigations. The donor-acceptor interactions of the DMH molecule were ascertained using the natural bond orbital (NBO). The mode of vibration was identified using the potential energy distribution (PED). An adaptation of the gauge independent atomic orbital (GIAO) method was used to assess the ^{1}H and ^{13}C NMR. The electronic transition of the molecule was confirmed using the time-dependent density functional theory (TD-DFT) approach. All the spectral analyses were compared theoretically and experimentally to bolster the goal of the findings. The theoretical band gaps were also predicted to be 4.26 eV, a vast energy gap suggesting the stability of the compound. In order to investigate the active area, the charge distribution and molecular electrostatic potential of DMH molecule were also investigated. Furthermore, the molecular docking was performed against three different proteins to examine the inhibition rate of the synthesized molecule.

Keywords: Pyrazole derivative, Morpholine, Piperidine, DFT, Electron-hole distribution, Docking studies, NLO.

INTRODUCTION

In pharmaceutical research, morpholine (tetrahydro-1,4-oxazine) is a well-known heterocyclic compound recognized for its favourable pharmacological, physicochemical and metabolic properties, as well as its remarkably straightforward synthesis. Numerous pharmacological effects such as analgesic, anti-inflammatory, antioxidant, anti-obesity, antihyperlipidemic, antibacterial, anti-neurodegenerative and anticancer activities, are exhibited by appropriately substituted morpholines [1-3]. Preluding, the first morpholine-containing medication to be sold, was first used to treat obesity in 1955 [1]. Two years later, a number of strong analgesics that were analogs of morpholine were developed. Since then, great strides have been made in investigating the entire range of biological roles of compounds containing morpholine, resulting in a sizable number of drugs that are currently on the market [2,4].

The increase in mortality and indisposition brought on by different pathogenic bacteria makes the quest for novel antimicrobial drugs an urgent problem. Multidrug-resistant microbial strains are becoming more and more common, which is a serious worldwide problem. At least one widely used antibiotic is ineffective against about 70% of bacterial infections [5]. Developing compounds with antimicrobial qualities by adding amino moieties and methoxy groups, which can alter their chemical makeup and boost biological activity, is one of the intriguing strategy [6]. Furthermore, aromatic rings are essential structural components of a large number of synthetic medications and physiologically active substances [7,8]. In this work, functionalized substituted amine compounds such as novel morpholine and piperidine derivatives based on 1-chloro-3-methoxy-propylbenzene, are synthesized and their antibacterial qualities assessed.

The synthesis, molecular docking analysis, anticancer efficacy and characterization of morpholine derivatives are reported in this work. Another crucial scaffold in the drug development is pyrazole, a five-membered heterocyclic molecule containing two nearby nitrogen atoms. Because of their

many biological characteristics, pyrazole derivatives are widely employed in therapeutics [9-11]. They are the building blocks of several drugs used to treat ailments like pain, bacterial infections, viral disorders, cancer and inflammation. Pyrazole derivatives are employed in producing metal-organic frameworks, coordination complexes and polymers in addition to medicines [12]. These materials have various applications, including catalysis, gas storage, sensing and drug delivery [13,14].

Understanding the electrical characteristics and reactivity of pyrazole derivatives now requires theoretical investigations employing density functional theory (DFT) and experimental assessments. DFT calculations help with the logical design of molecules with better biological properties by revealing the information about molecular orbitals, electronic band gaps, charge distribution and possible interaction locations. The goal of this study is to better understand the structure-activity correlations of pyrazole derivatives by integrating computational studies with experimental data. This study aims to explore the synthesis, biological evaluation and theoretical calculations of pyrazole derivative *viz*. 4-(4,5-dihydro-3-(4-morpholinophenyl)-1*H*-pyrazol-5-yl)-*N*,*N*-dimethylbenzenamine (DMH), focusing on their potential as drugs in the biological applications.

EXPERIMENTAL

Synthesis of 4-(4,5-dihydro-3-(4-morpholino-phenyl)-1*H*-pyrazol-5-yl)-*N*,*N*-dimethylbenzenamine (DMH): A beaker containing 1-(4-morpholinophenyl)ethanone (5 mmol) and 4-(dimethylamino)benzaldehyde (5 mmol) were dissolved in ice-cold ethanol at 20 ºC followed by the addition of NaOH solution (15 mmol) while keeping the temperature constant. The reaction was halted with ice-cold water and allowed to mature overnight following 6 h of stirring and TLC monitoring. To obtain 3-(4-(dimethylamino)phenyl)-1-(4-morpholinophenyl)-prop-2-en-1-one (chalcone), the solid product was filtered, washed with distilled water and then dried under vacuum. In the next step, chalcone (1 mmol) was mixed with hydrazine hydrate (3 mmol), NaOH solution and ethanol, then stirred at room temperature for 8 h. After TLC confirmation, the reaction was quenched with ice and then the solid product was filtered, washed with distilled water and then dried *in vacuo* to obtain 4-(4,5-dihydro-3-(4-morpholinophenyl)-1*H*-pyrazol-5-yl)-*N*,*N*-dimethylbenzenamine (**Scheme-I**).

Characterization: The UV-Vis spectra were recorded using a SpectraMax Plus 384 spectrophotometer (molecular devices). The sample was dissolved in methanol, and its absorption spectrum was recorded to determine the maximum absorption wavelength (λ_{max}). FT-IR spectra were measured using a Bruker FT-IR spectrometer. The sample was mixed with KBr, pressed into a pellet and analyzed. A BRUKER AMX-400 spectrometer running at 400 MHz for ^{1}H NMR and 100 MHz for ^{13}C NMR with $CDCl_3$ as solvent was used to perform the structural confirmation using ^{1}H and ^{13}C NMR spectroscopy at 293 K. The chemical shifts (δ) were reported in ppm relative to TMS as an internal reference and measurements were made using 5 mm NMR tubes.

Computational details: The geometrical parameters for the DMH molecule were evaluated by Gaussian 09W software with B3LYP/6-311G (d, p) basis set/functional group. GaussView 5.0.1 software designed for stable structure [15,16]. The optimized structure also predicted the mode of vibrations to ensure the global minima. The nucleophilic and electrophilic states of the titled molecule were ascertained by using molecular electrostatic potential studies. The reactive nature was also predicted by the HOMO and LUMO analysis using the GaussSum package [17]. Docking studies were conducted using Autodock Vina software to evaluate the biological activity of the titled molecule [18]. Theoretical UV-Vis spectra and FT-IR analysis were also employed and correlated with the experimental data.

RESULTS AND DISCUSSION

Structural analysis: Molecular structure determination enables the identification of functional sites, charge transfer characteristics and electrostatic potential, all of which are essential for accurate computational modeling and interaction prediction. The lowest energy state of the titled molecule is optimized through quantum mechanical calculations using the DFT embedded in Gaussian 09W software. The lowest energy state of DMH molecule was computed using B3LYP functional and basis set of 6-311(d,p) [19]. The results show

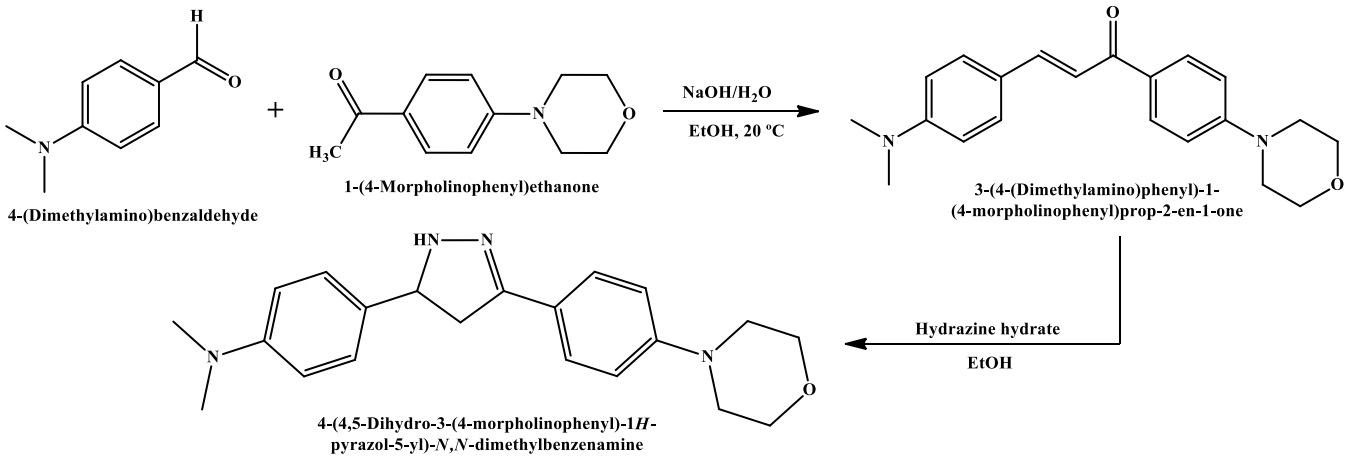

Scheme-I: Synthesis procedure of 4-(4,5-dihydro-3-(4-morpholinophenyl)-1*H*-pyrazol-5-yl)-*N*,*N*-dimethylbenzenamine (DMH)

the energy of the optimized structure at the stable position is -40.8 eV and the estimated dipole moment is 3.275 Debye. Therefore, energy moves from right to left, *i.e.* from the morpholino phenyl to dimethylbenzylamine. The optimized structure of the molecule is shown in Fig. 1 and the bond-lengths are tabulated in Table-1.

TABLE-1
OPTIMIZED BOND LENGTH (Å) AND BOND ANGLE (º) OF DMH MOLECULE

Bond length	Values (Å)	Bond angle	Values (º)	Bond angle	Values (º)
C1-C2	1.3932	C2-C1-C6	121.0179	H24-C23-H26	107.9891
C1-C6	1.4028	C2-C1-H7	118.4906	H25-C23-H26	108.2528
C1-H7	1.0815	C6-C1-H7	120.4855	C15-C28-C29	116.5507
C2-C3	1.3978	C1-C2-C3	121.6559	C15-C28-N31	113.4166
C2-H8	1.0841	C1-C2-H8	118.3944	C15-C28-H34	108.7138
C3-C4	1.4079	C3-C2-H8	119.9415	C29-C28-N31	100.0051
C3-C30	1.4625	C2-C3-C4	117.2683	C29-C28-H34	107.9188
C4-C5	1.3804	C2-C3-C30	121.5819	N31-C28-H34	109.8351
C4-H9	1.083	C4-C3-C30	121.1491	C28-C29-C30	100.6371
C5-C6	1.412	C3-C4=C5	121.3784	C28-C29-H35	111.1147
C5-H10	1.0829	C3-C4-H9	118.5549	C28-C29-H36	112.5086
C6-N41	1.408	C5=C4-H9	120.0611	C30-C29-H35	110.4595
C11-C12	1.4106	C4=C5-C6	121.4251	C30-C29-H36	114.2057
C11-C16)	1.3902	C4=C5-H10	118.8127	H35-C29-H36	107.8525
C11-H17	1.0811	C6-C5-H10	119.7343	C3-C30-C29	125.4369
C12-C13	1.4127	C1-C6-C5	117.2488	C3-C30-N32	122.4723
C12-H21	1.3896	AC1-C6-N41	122.5856	C29-C30=N32	112.0005
C13-C14	1.3877	C5-C6-N41	120.1316	C28--N31-N32	109.2351
C13-H18	1.0811	C12-C11-C16	120.9276	C28-N31-H33	115.2646
C14-C15	1.398	C12-C11-H17	120.4819	N32-N31-H33	110.3957
C14-H19	1.0839	C16-C11-H17	118.5893	C30=N32-N31	109.2744
C15-C16	1.3953	C11-C12-C13	116.943	C38-C37-N41	109.8509
C15-C28	1.51	C11-C12-N21	121.5906	C38-C37-H43	108.6314
C16-H20	1.0863	C13-C12-N21	121.4661	C38-C37-H44	109.2188
N21-C22	1.4526	C12-C13-C14	121.2411	N41-C37-H43	109.2087
N21-C23	1.453	C12-C13-H18	120.3271	N41-C37-H44	111.7542
C22-H27	1.0896	C14-C13-H18	118.4309	H43-C37-H44	108.1091
C22-H50	1.1008	C13-C14-C15	121.6182	C37-C38-O42	111.8093
C22-H51	1.0938	C13-C14-H19	119.3713	C37-C38-H45	109.3372
C23-H24	1.0936	C15-C14-H19	118.9921	C37-C38-H46	110.2678
C23-H25	1.0896	C14-C15-C16	117.3032	O42-C38-H45	109.9681
C23-H26	1.1006	C14-C15-C28	121.7757	O42-C38-H46	106.5806
C28-C29	1.5457	C16-C15-C28	120.9133	H45-C38-H46	108.8083
C28-N31	1.4821	C11-C16-C15	121.9398	C40-C39-N41	110.1792
C28-H34	1.1014	C11-C16-H20	118.5884	C40-C39-H48	109.2059
C29-C30	1.5201	C15-C16,20	119.4703	C40-C39-H49	109.1928
C29-H35	1.097	C12-N21-C22	119.299	N41-C39-H48	110.4064
C29-H36	1.0906	C12-N21-C23	119.3069	N41-C39-H49	110.0815
C30=N32	1.289	C22-N21-C23	117.5522	H48-C39-H49	107.7263
N31-N32	1.3905	N21-C22-H27	109.015	C39-C40-O42	111.3546
N31-H33	1.0127	AN21-C22-H50	113.0328	C39-C40-H47	110.401
C37-C38	1.5269	N21-C22-H51	111.008	C39-C40-H52	109.5888
C37-N41	1.4602	H27-C22-H50	108.2555	O42-C40-H47	106.569
C3-H43	1.0921	H27-C22-H51	107.3572	O42-C40-H52	109.968
C37-H44	1.1037	H50-C22-H51	107.9823	H47-C40-H52	108.8929
C38-O42	1.42	N21-C23-H24	111.0146	C6-N41-C37	118.3812
C38-H45	1.1005	N21-C23-H25	109.0072	C6-N41-C39	117.8514
C38-H46	1.0915	N21-C23-H26	113.0233	C37-N41-C39	111.5829
C39-C40	1.5242	H24-C23-H25	107.3645	C38-O42-C40	110.456
C39-N41	1.4689				
C39-H48	1.1029				
C39-H49	1.0893				
C40-O42	1.421				
C40-H47	1.0915				
C40-H52	1.1006				

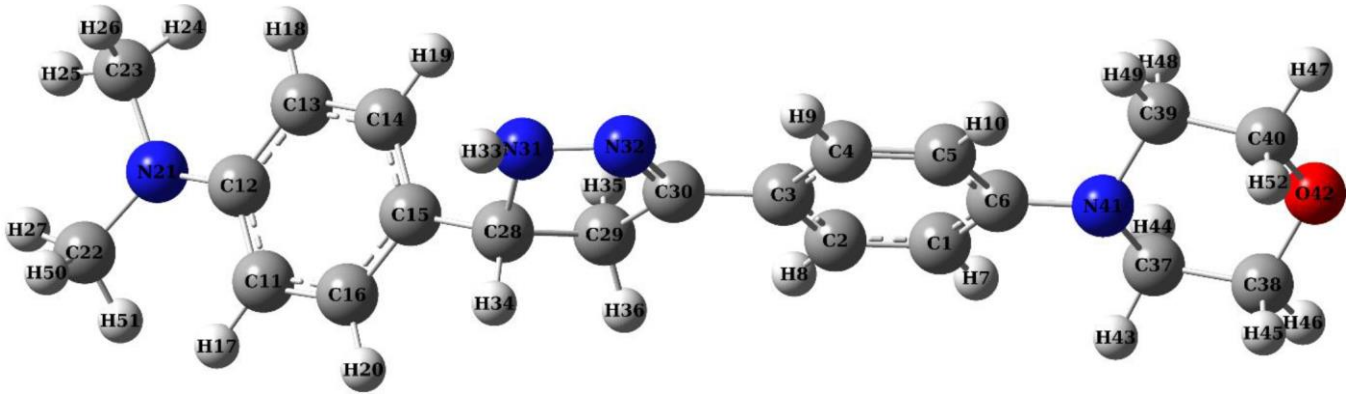

Fig. 1. Optimized structure of 4-(4,5-dihydro-3-(4-morpholinophenyl)-1*H*-pyrazol-5-yl)-*N*,*N*-dimethylbenzenamine (DMH)

The molecular bond lengths are as follows: C–C is ~1.50 Å in pyrazole and ~1.39 Å in benzene rings; C–O ranges from 1.38–1.42 Å; C–H is 1.06–1.09 Å; N–H is ~1.02 Å; C–N is ~1.43 Å; C=N is ~1.38 Å; and N–N is ~1.12 Å [20-22]. Some parts of the target molecule deviate from the original structure, while other regions stabilize through the uniformity of bond lengths between adjacent functional groups. Similarly, the C–C, N–H and C–O bond lengths remain consistent throughout the titled molecule. However, due to the attachment of the C=C bond to the nitrogen atom, more significant variations up to 0.02 Å are observed at the C12–C13 position. Once stabilized through interactions with nearby atoms, the C3–C4 and C1–C8 bonds likewise exhibit minimal variation, limited to about 0.01 Å. On the other hand, C-N shortens with values of 0.04 Å at C12-C21 and elongates with a distance of 0.05 Å at one point (C28-N31). Similarly, N-N elongates itself by 0.027 Å and accepts the higher values. According to the literature, it maintains its initial bond lengths in every other molecular region [23].

In terms of bond angles, some deviations are observed in the optimized structure. Generally, the internal angles of the benzene rings remain close to 120º, reflecting their aromatic character. However, in certain regions, slight deviations occur due to the influence of the surrounding molecular environment. In the titled compound, the angles C2–C1–C6 and C1–C2–C3 deviate by approximately 1.0º to 1.6º, while the C1–C6–C5 angle contracts to 117º, showing a reduction of about 3º [24]. The bond angles within the other rings remain consistent with values reported in the literature

Experimental FT-IR: A prominent absorption band at 1598 cm^{-1}, corresponding to C=N stretching, is observed in the FT-IR spectrum of the synthesized compound. Aromatic and aliphatic C-H stretching are responsible for the absorption bands at 2959 cm^{-1} and 2859 cm^{-1}, respectively. C-O stretching is represented by a peak at 1189 cm^{-1}, whereas the peak at 1231 cm^{-1} represents the C-N stretching [25]. These characteristic vibrational frequencies confirm the successful synthesis of the titled compound. The sharp vibrating peaks were observed in Fig. 2a.

Theoretical FT-IR analysis: Infrared absorption arises from changes in the dipole moment of a molecule, indicating the presence of specific functional groups. Vibrational analysis was employed to identify the corresponding molecular vibration modes. The theoretical FT-IR spectra were depicted in Fig. 2b. The 52-atom DMH molecule exhibits 150 vibrational modes, calculated using the non-linear molecule formula 3n-6. The molecular symmetry is in good agreement with the reference data (Table-2), since it belongs to the C_1 point group [26]. The VEDA software was used to acquire total energy distribution (TED) data, which were then used to determine the vibrational assignments [27].

CH vibrations: The titled molecule exhibits strong electronic delocalization, primarily due to the presence of two six-membered aromatic rings. The dimethylbenzenamine, pyrazole, and morpholine rings of the compound exhibit CH vibrations around 3071, 3053, 3022, 2989, and 2859 cm^{-1}. Among these bands, the sharp peaks at 3071 and 3052 cm^{-1} correspond to the CH stretching vibrations [28].

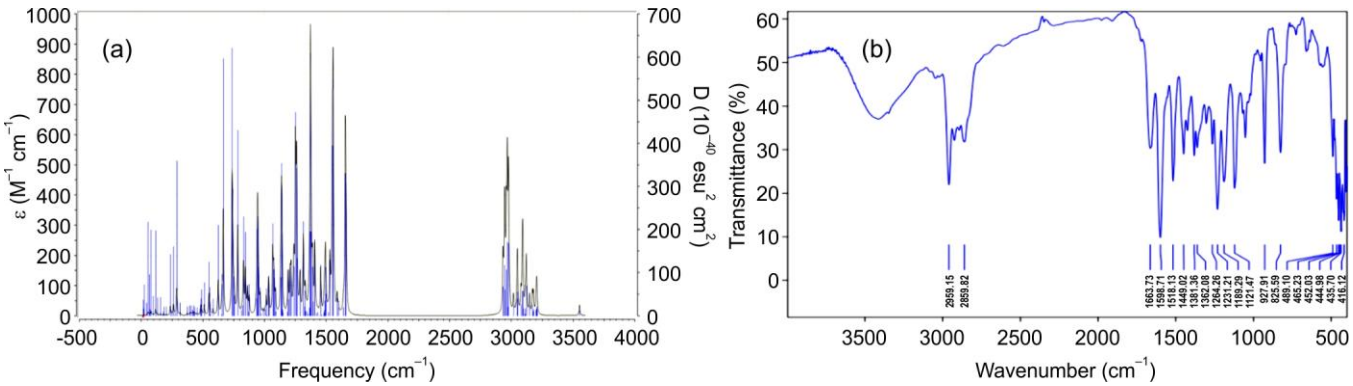

Fig. 2. Theoretical (a) and experimental (b) FT-IR spectra of DMH

TABLE-2
VIBRATIONAL ASSIGNMENTS OF DMH MOLECULE

Mode Nos.	Unscaled	Scaled	IR_{int}	TED Assignments
1	3553.9244	3411.767424	10.4534	
2	3206.6808	3078.413568	12.2487	
3	3206.6808	3078.413568	3206.6808	
4	3203.7827	3075.631392	12.677	
5	3199.3391	3071.365536	3199.3391	ν CH (97)
6	3180.5112	3053.290752	11.9631	ν CH (91)
7	3179.7645	3052.57392	7.7412	
8	3171.8464	3044.972544	20.53	
9	3148.417	3022.48032	18.5629	ν CH (97)
10	3122.7449	2997.835104	54.0931	
11	3114.3007	2989.728672	12.9104	ν CH (97)
12	3110.6302	2986.204992	2.7996	
13	3097.2423	2973.352608	13.2801	ν CH (94)
14	3093.4101	2969.673696	44.4004	ν CH (30)
15	3091.3462	2967.692352	43.925	ν CH (66)
16	3079.1435	2955.97776	19.8013	ν CH (96)
17	3051.2334	2929.184064	42.3263	ν CH (82)
18	3048.0636	2926.141056	30.5198	ν NC (15)
19	3017.9694	2897.250624	17.0342	ν CH (76)
20	2979.0357	2859.874272	125.2732	ν CH (44)
21	2973.1988	2854.270848	14.77	ν CH (49)
22	2968.4791	2849.739936	127.6917	
23	2960.4904	2842.070784	78.9471	
24	2949.9829	2831.983584	44.6711	
25	2945.6275	2827.8024	86.6551	
26	2934.0791	2816.715936	49.7473	ν CH (90)
27	1659.7611	1593.370656	128.2668	
28	1654.7732	1588.582272	136.983	
29	1640.1101	1574.505696	7.8551	ν NC (62)
30	1600.362	1536.34752	7.5292	ν CC (29)
31	1589.5509	1525.968864	16.4287	
32	1556.971	1494.69216	214.2603	
33	1550.1923	1488.184608	153.3585	β HCC (11)
34	1531.4191	1470.162336	49.8348	β HCH (11)
35	1516.0836	1455.440256	2.8821	β HCH (33)
36	1500.3689	1440.354144	19.2298	β HCH (12)
37	1493.5665	1433.82384	14.5473	β HCH (21)
38	1493.4152	1433.678592	42.0459	β HCH (14)
39	1488.1431	1428.617376	13.0955	β HCH (15)
40	1486.0823	1426.639008	0.6611	β HCH (12)
41	1485.1051	1425.700896	4.7376	γ CHNH (68) + γ CHNH (10)
42	1483.5331	1424.191776	0.401	
43	1481.2475	1421.9976	2.624	β HCH (82)
44	1464.0152	1405.454592	0.5632	ν CC (34)
45	1456.4494	1398.191424	42.9477	ν CC (43) + β HCH (14)
46	1446.9426	1389.064896	0.3778	
47	1432.621	1375.31616	2.9955	
48	1422.0381	1365.156576	2.1926	τ HCOC (60)
49	1408.9023	1352.546208	62.493	
50	1393.8953	1338.139488	11.4289	
51	1389.3549	1333.780704	1389.3549	β HCC (55)
52	1377.7664	1322.655744	67.3326	
53	1373.1539	1318.227744	209.3844	γ CHNH (10) + ν NC (33)
54	1369.3767	1314.601632	66.7999	ν CC (11) + β HCC (10)
55	1364.165	1309.5984	6.4173	τ HCNC (11) + τ HCOC (11)
56	1354.6622	1300.475712	1.5903	
57	1342.0296	1288.348416	3.2075	β HCC (62)
58	1333.1762	1279.849152	3.5166	β HCO (42)

59	1331.2614	1278.010944	19.4806	γ CCCH (10) + β HCO (20)
60	1325.054	1272.05184	6.9828	ν CC (12)
61	1315.4229	1262.805984	72.1614	γ CCCH (36)
62	1287.9183	1236.401568	34.9656	
63	1263.3622	1212.827712	41.8782	ν CC (18) + ν NC (30)
64	1260.1628	1209.756288	108.3358	β HCC (11) + τ HCCN (14)
65	1252.1231	1202.038176	148.3422	ν NC (12) + β HCN (11)
66	1239.6208	1190.035968	14.517	
67	1238.2037	1188.675552	35.3709	β HCO (33) + β HCN (28)
68	1215.2232	1166.614272	38.5872	β HCC (72)
69	1208.4416	1160.103936	33.5998	β HCC (50)
70	1194.8061	1147.013856	11.3708	
71	1191.4239	1143.766944	31.1119	γ CHNH (48)
72	1183.4413	1136.103648	2.5033	τ HCCN (19) + β HCC (29)
73	1150.4429	1104.425184	2.3532	ν CC (12) + β HCC (38)
74	1145.7707	1099.939872	3.9541	
75	1142.985	1097.2656	54.922	
76	1138.1084	1092.584064	101.0748	ν OC (65)
77	1133.5292	1088.188032	0.8476	
78	1132.3232	1087.030272	25.0678	γ CCNH (25) + τ COCC (21)
79	1090.3437	1046.729952	2.6095	β HCN (11) + γ CCNH (19)
80	1089.3755	1045.80048	16.2076	ν NN (28) + ν CC (12)
81	1078.6395	1035.49392	23.6837	
82	1074.4057	1031.429472	28.8243	β CNN (15) + ν NC (12) + ν CC (10)
83	1067.0007	1024.320672	57.2366	
84	1035.405	993.9888	11.9458	ν CC (26) + β COC (10)
85	1033.2337	991.904352	24.1669	ν NN (12)
86	1024.6669	983.680224	1024.6669	
87	1015.3105	974.69808	16.0342	β CCC (61
88	1005.0585	964.85616	1005.0585	γ CCCH (45)
89	989.1744	949.607424	4.0344	γ CCCH (58) + τ HCCN (27)
90	971.4994	932.639424	0.9867	
91	964.7753	926.184288	15.8065	
92	950.0489	912.046944	27.0573	ν CH (98) + τ HCCN (23) + τ HCCC (34)
93	946.0877	908.244192	25.128	τ HCCC (12) + γ CCCH (46) + ν CH (89)
94	945.3928	907.577088	54.5716	
95	941.673	904.00608	47.3723	
96	933.9135	896.55696	9.3386	
97	876.2845	841.23312	15.9255	β CCN (21) + ν CC (14) + ν NC (15)
98	870.7365	835.90704	1.8721	
99	862.8482	828.334272	10.9554	β CNN (25) + ν CC (29) + ν CC (11)
100	862.1479	827.661984	12.3804	β CNN (25) + ν CC (29) + ν CC (11)
101	846.4335	812.57616	41.22	τ HCCN (46) + γ CCCH (11)
102	830.7192	797.490432	47.8887	
103	822.6674	789.760704	4.8486	
104	813.8184	781.265664	2.5916	
105	783.6989	752.350944	84.4791	
106	756.464	726.20544	8.7866	β CCC (13)
107	751.3402	721.286592	17.2811	τ CCCC (18) + γ NCCC (16) + γ CCCC (12)
108	743.2342	713.504832	54.8552	β CCC (14) + γ NCNH (10)
109	738.3914	708.855744	114.9707	γ NCNH (16) + τ CCCC (15) + γ NCCC (12)
110	666.6606	639.994176	99.654	
111	655.8551	629.620896	15.773	ν CC (31)
112	651.9064	625.830144	0.4974	
113	624.7755	599.78448	32.8622	
114	583.2892	559.957632	5.7751	β CCC (15) + τ CNNC (15)
115	559.533	537.15168	0.5464	
116	555.4805	533.26128	9.2097	γ NCCC (23) + γ CCCC (18)
117	551.0736	529.030656	17.2089	γ NCCC (36) + γ CCCC (19)
118	512.6874	492.179904	9.9644	
119	489.2202	469.651392	7.4489	β CCO (10) + β CCN (12)

120	484.2373	464.867808	4.83	β HCH (85) + β CCN (11) + β CCC (10)
121	480.6871	461.459616	2.8724	
122	452.9796	434.860416	2.2345	
123	436.3134	418.860864	2.1991	β CCN (12)
124	427.6053	410.501088	0.9047	
125	424.3284	407.355264	2.5514	τ CCCC (78)
126	417.0474	400.365504	1.3659	τ CCCC (15)
127	405.8357	389.602272	2.4234	
128	395.4794	379.660224	2.3287	τ CCCC (17)
129	373.5635	358.62096	1.9903	ν NC (66) + γ CHNH (10)
130	316.7411	304.071456	2.4055	
131	289.7111	278.122656	26.1036	
132	274.3825	263.4072	0.4617	τ HCNC (12)
133	262.6581	252.151776	10.5536	
134	249.8892	239.893632	0.6772	
135	237.5165	228.01584	8.4475	
136	205.4873	197.267808	1.0651	τ HCNC (44)
137	185.6533	178.227168	0.9955	
138	178.3732	171.238272	0.4159	τ HCNC (15)
139	157.5039	151.203744	1.7051	β CCC (14) + β CCN (13) + τ HCNC (11)
140	133.2942	127.962432	1.4104	γ NCCC (11)
141	118.3771	113.642016	5.857	γ NCCC (40)
142	96.6738	92.806848	96.6738	
143	81.0173	77.776608	4.0492	τ CCCN (12)
144	72.298	69.40608	0.2703	τ CCNC (59)
145	67.667	64.96032	1.6266	
146	57.4867	55.187232	3.1436	
147	44.5765	42.79344	0.3362	
148	24.2261	23.257056	0.4378	τ CCCN (31) + τ CCCC (20) + τ CCNC (10)
149	19.3079	18.535584	0.0767	
150	16.1402	15.494592	0.1507	

C=C vibration: The ring membrane often exhibits the C=C vibration at 1536, 1405 cm^{-1}, which is consistent with the experimental range. A slight constrain in the wavelength was due to nearby pyrazole. The theoretical and experimental FT-IR spectra shown in Fig. 2a-b exhibit sharp peaks at the same positions, indicating that the theoretical results closely match the experimental data.

UV-Vis spectral analysis: Both the experimental and theoretical UV-Vis studies confirm the presence of π→π* transition corresponding to the conjugated carbonyl groups in the molecule. A shoulder peak at 359 nm was due to the presence of conjugation between the aromatic ring and the carbonyl group [29]. The peak at 300 nm corresponds to the π-π* of the ligand molecule. The experimental and theoretical analyses are in good agreement. However, a slight shift was observed in the theoretical analysis due to the TD-DFT method. The experimental and theoretical absorbance peaks are shown in Fig. 3a-b. A subtle change in the peak was observed due to the exchange-correlation function. Further, the energy gap and the chemical stability were derived from the FMO studies. The HOMO and LUMO values also validated the strong electron-donating character, which can facilitate π→π* transitions. The energy gap suggests a wider band gap and acts as an electronic application and NLO property.

^{1}H NMR analysis: The four numbers of the two sets of N-CH_2 protons of the morpholine ring are responsible for the signal that occurred at 3.20-3.32 ppm in the ^{1}H NMR spectrum of the titled compound. Similarly, the four numbers of the two sets of O-CH_2 protons of the morpholine ring are responsible for the signal that emerged around 3.85-3.86 ppm. The six protons of the two CH_3 groups affixed to the nitrogen atom of the dimethylamino portion connected to the aromatic ring are responsible for the signal detected at 2.89-2.96 ppm. At 2.89-2.96 ppm, the signals for the pyrazolyl ring's three aliphatic C-H protons are combined and detected [30]. The phenyl rings' aromatic protons were found between 6.73 and 8.02 ppm (Fig. 4a).

^{13}C NMR analysis: The two carbons bonded to the nitrogen atom in the morpholine ring are responsible for the signal seen at 48.14-48.94 ppm in the ^{13}C NMR spectrum of titled compound. The two carbons bonded to the oxygen atom in the morpholine ring are also responsible for the signal observed at 56.52-56.82 ppm. The carbon signal observed at 47.34-47.55 ppm is attributed to the two methyl carbons bonded to the nitrogen atom of the dimethylamino group attached to the aromatic ring [31]. The signal observed at 46.57 ppm is due to the N-C carbon in the pyrazolyl ring whereas the signal observed at 70.16 ppm is due to the N=C carbon in the pyrazolyl ring. The signal at 33.84 ppm corresponds to the aliphatic –CH_2 carbon within the pyrazolyl ring. The two phenyl rings' aromatic carbons were found between 113.18 and 130.30 ppm, whereas the aromatic *ipso*-carbons were found between 148.26 and 154.54 ppm [32] (Fig. 4b). The ^{13}C NMR data of the synthesized compound provide further evidence for the successful formation of the DMH compound.

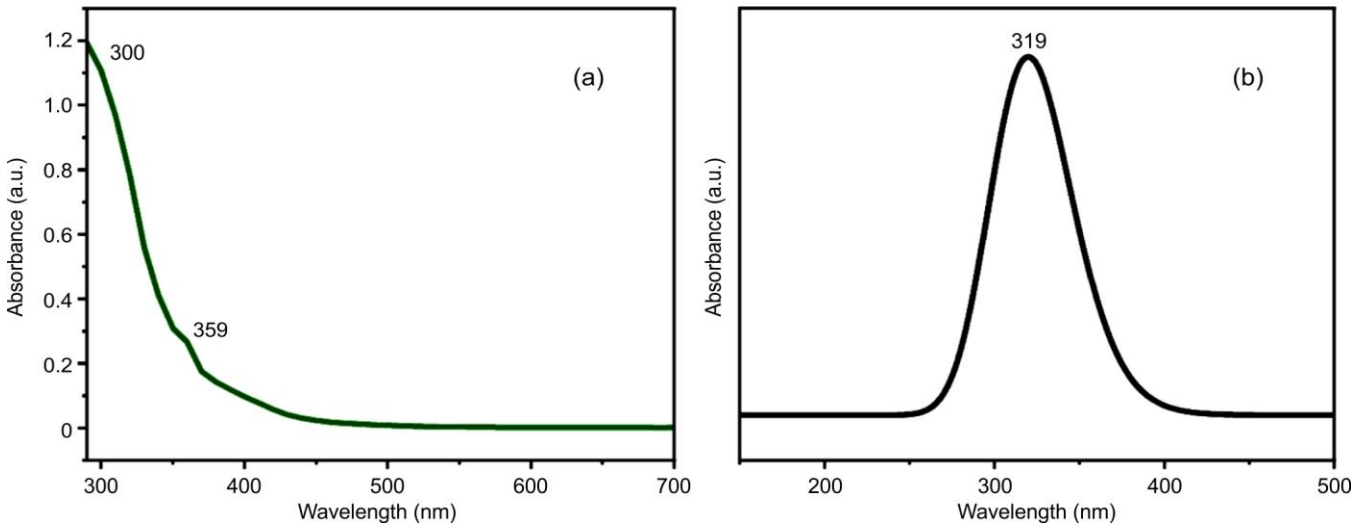

Fig. 3. Experimental (a) and theoretical (b) UV-Vis spectra of DMH

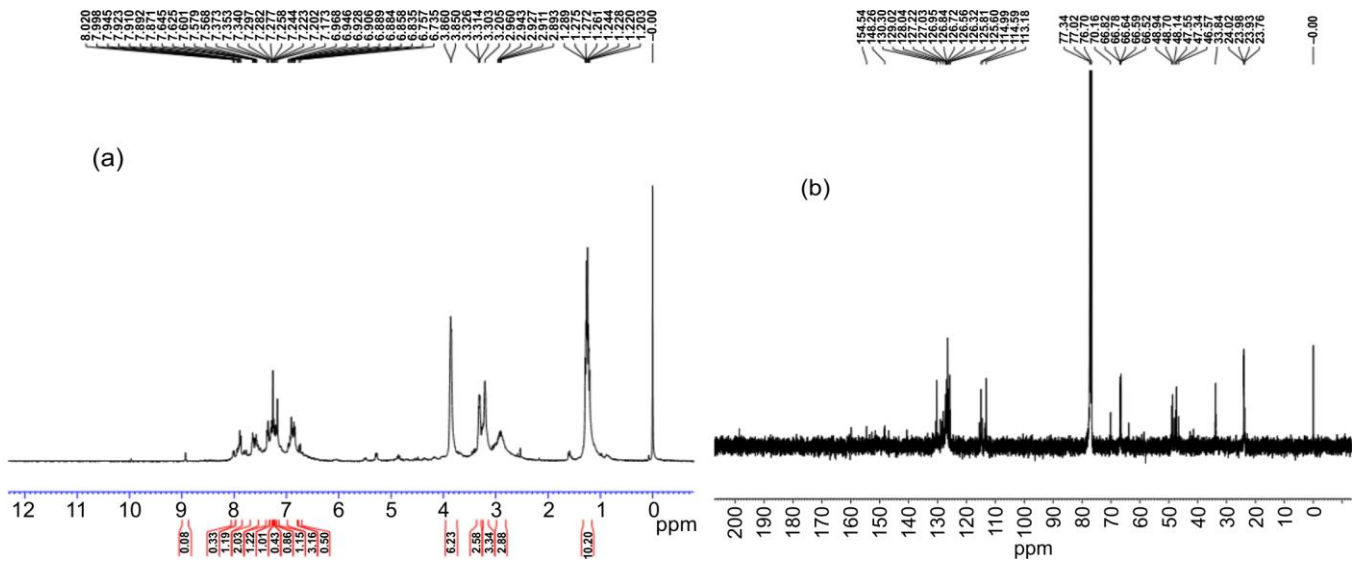

Fig. 4. ^{1}H NMR (a) and ^{13}C NMR (b) spectra of DMH

The nitrogen atom bonded with the two carbons in the morpholine ring are responsible for the signal at 48.14-48.94 ppm in the ^{13}C NMR spectrum of DMH compound [33]. In the pyrazolyl ring, the N-C carbon is responsible for the signal detected at 46.57 ppm, whereas the N=C carbon is responsible for the signal at 70.16 ppm. The aliphatic -CH_2 carbon in the pyrazolyl ring is the cause of the signal at 33.84 ppm. The aromatic carbons of the two phenyl rings were observed between 113.18 and 130.30 ppm, while the aromatic *ipso*-carbons appeared in the range of 148.26 to 154.54 ppm. The ^{13}C NMR data further validates the synthesis of the oxygen atom attached with the two carbons atoms in the morpholine ring are also responsible for the signal at 56.52-56.82 ppm. Another carbon signal observed at 47.34–47.55 ppm is attributed to the two methyl carbons bonded to the nitrogen atom in the molecule (Fig. 4b).

Theoretical NMR analysis

^{1}H NMR analysis: The aromatic hydrogen atoms are influenced by the anisotropic effect of the aromatic ring current, leading to deshielding and resulting in proton signals appearing in the 7–8 ppm region of the ^{1}H NMR spectrum. This is characteristic of protons located on conjugated aromatic systems, such as those found in phenyl and heteroaromatic rings. The wide or numerous peaks in the 5-6 ppm range might be signs of alkene protons (C=CH) or vinyl. Protons connected to heteroatoms are frequently attributed to the chemical changes in the 2-4 ppm range [34] (Fig. 5a). The –CH_3, –CH_2– and –CH groups usually belong to the upfield area (2-0 ppm).

^{13}C NMR analysis: In aromatic or conjugated systems, the downfield (high δ value) peaks in the 150-100 ppm range most likely belong to sp^2 hybridized carbons. The carbonyl (C=O) or conjugated carbons, which are significantly deshielded by electronegative oxygen, may be represented by the peaks at 170-160 ppm. The C=C double bonds of aromatic ring are indicated by the peaks at 120-100 ppm (Fig. 5b). The sp^2 hybridized carbon atoms bound to electronegative elements like nitrogen or oxygen may be responsible for the peaks in the 60-40 ppm range.

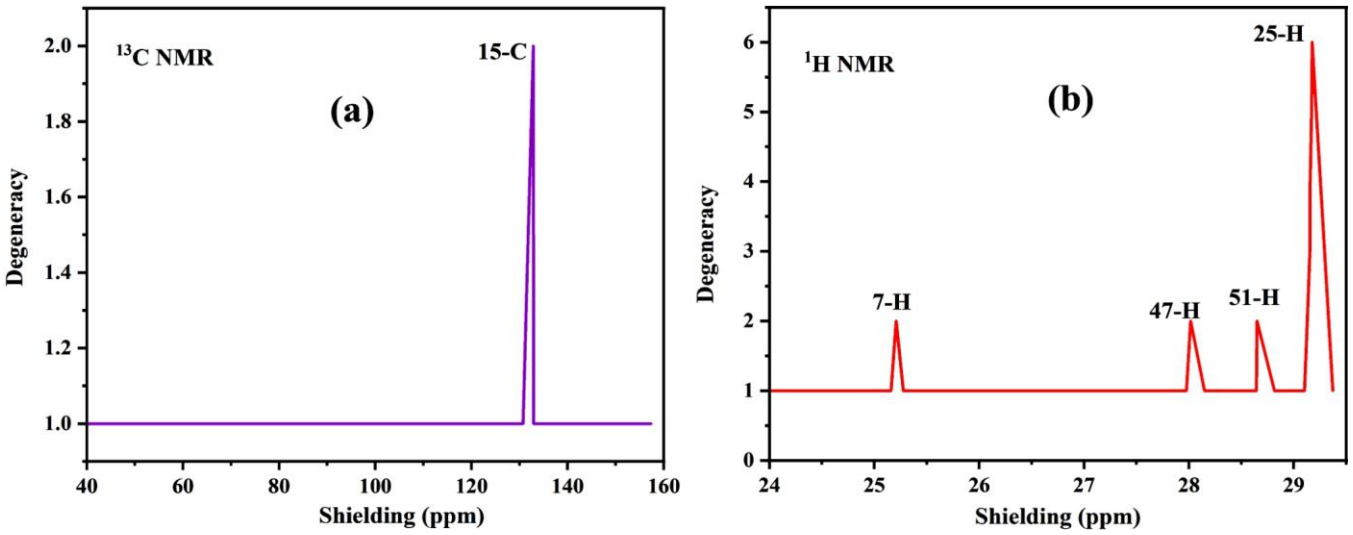

Fig. 5. Theoretical ^{13}C NMR (a) and ^{1}H NMR (b) spectra of DMH

Comparative NMR analysis

Strong consistency may be shown in aromatic ^{13}C shifts (160-100 ppm) and ^{1}H shifts (7-9 ppm). Both spectra show the electronegative effects (C-O or C-N in the 70–80 ppm area). The presence of anticipated functional groups is confirmed by the agreement between theoretical and experimental results [35]. The structural validity of the synthesized molecule is confirmed by the good alignment of the experimental and DFT-calculated NMR spectra. The observed shifts in both spectra support the presence of electronegative substituents, conjugation effects, and aromatic rings.

Molecular electrostatic potential (MEP): This study also presents the physico-chemical properties of the titled molecule, including its electrophilic and nucleophilic characteristics, as well as its potential in drug design modeling. The MEP map and contour plot of the titled molecule are shown in Fig. 6, whereas the colours red, blue, yellow and green represent regions of electron richness, electron deficiency, slight electron richness and neutral potential, respectively [36]. The MEP colour contour indicates that the positive zone, also known as the nucleophilic region, is located over the hydrogen atom, while the negative sections are electrophilic and primarily include the region of oxygen and nitrogen atoms. These observations indicate that the N and O atoms correspond to regions of highest electron density, acting as centers of electron repulsion, whereas the hydrogen atoms exhibit pronounced electron deficiency, reflecting areas of strong electrophilic attraction. Furthermore, the electron density plot demonstrates a relatively uniform distribution of electron density across the entire molecular framework, highlighting the overall electronic stability of DMH molecule.

HOMO–LUMO reactivity: The HOMO–LUMO energy gap is a key parameter indicating the chemical reactivity and stability of the molecule [37]. The HOMO and LUMO energies of the titled molecule were found to be –5.04 eV and –0.78 eV, respectively, resulting in a HOMO–LUMO gap of 4.26 eV, which indicates the moderate chemical reactivity [38] (Fig. 7). The electronegativity and the electrophilicity index, which accounts for the number of electrons attracted towards

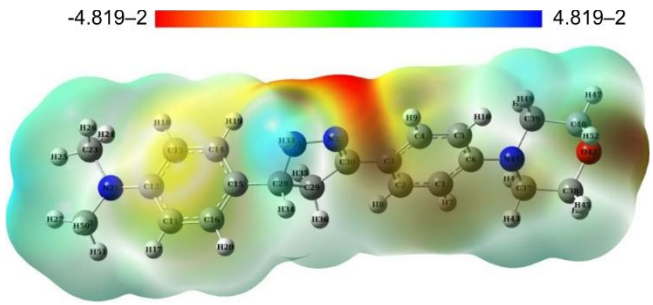

Fig. 6. MEP colour mapping of DMH molecule

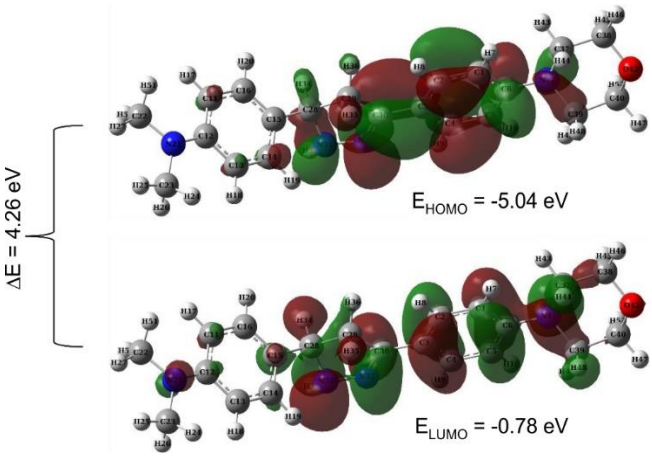

Fig. 7. HOMO LUMO orbital composition of DMH molecule

the molecule, is 2.91 eV. The chemical hardness and the chemical softness of the molecules were calculated and shown in Table-3.

Electron-hole analysis: The first excited state (S1) denotes the shift of one donor to another, indicating the $\pi \rightarrow \pi^*$. Fig. 8 suggests strong delocalization over conjugated carbon atoms in the benzene structure of the molecule. The second excited state (S2) proposes a charge transfer from pyrazole to the morpholine ring or the morpholine to the pyrazole ring in a *vice-versa* manner, which results in the molecular excitation. State of third excitation (S3) A higher energetic transition is

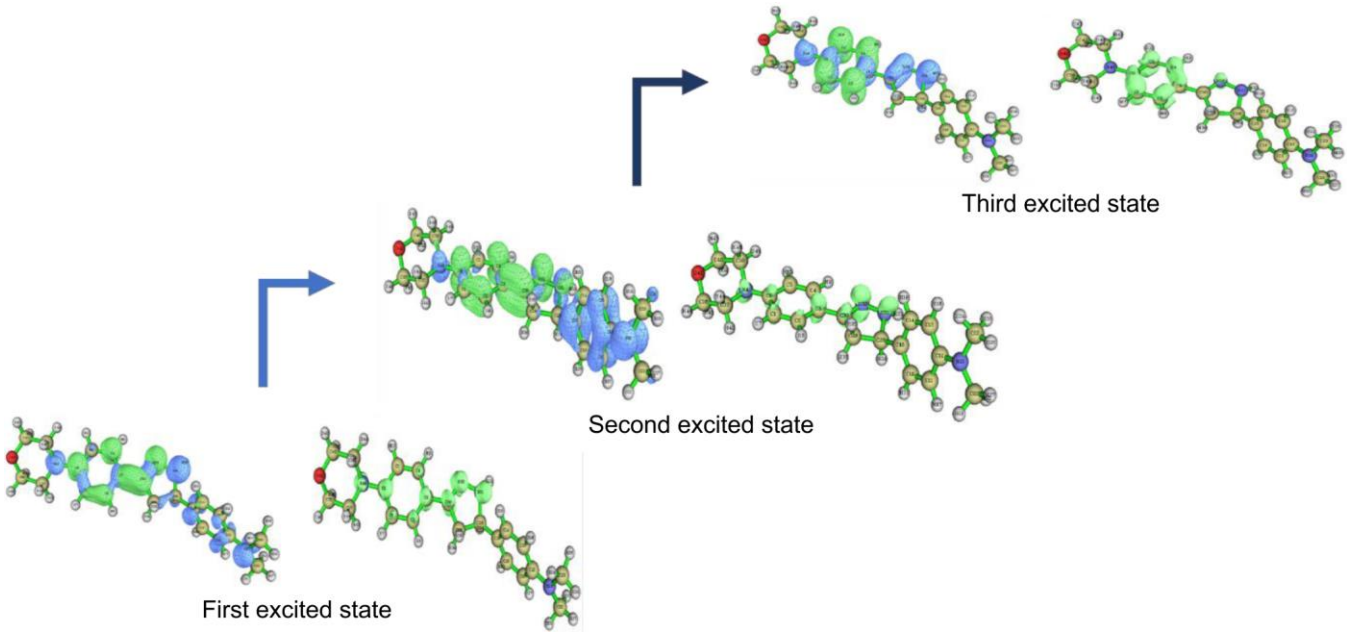

Fig. 8. Electron-hole distribution and electron-hole overlap for three excited states of DMH molecule

TABLE-3
HOMO LUMO REACTIVE DESCRIPTOR ANALYSIS

Parameters	Values
E_{HOMO} (eV)	-5.04
E_{LOMO} (eV)	-0.78
$E_{HOMO} - E_{LOMO}$ gap (eV)	-4.26
Ionization potential (I)	5.04
Electronegativity (χ)	2.91
Electron affinity (A)	0.78
Global hardness (η)	2.13
Chemical potential (μ)	-2.91
Electrophilicity index (ω)	1.12584507
Global softness (S)	0.234741784

probably represented by the electron density's apparent high dispersion. Further delocalization or perhaps a mixed n→π and π→π** excitation involving non-bonding orbitals could be indicated by this notation [39]. These electronic transitions were predicted through the experimental UV-Vis analysis at 300 nm. These results suggest the molecule has nonlinear optical properties.

NLO properties: The dipole, first hyperpolarizability and quadrupole were calculated from the theoretical aspects. The dipole moment of the titled molecule was determined to be 1.1009 D, which shows its vibrational behaviour. The anisotropy and quadrupole values are 266.76 a.u. and 15.38 a.u., suggesting a strong optical application. The calculated first hyperpolarizability (β = 154.79 a.u.) indicates that the pyrazole derivative exhibits a reasonable NLO property compared with the standard references [40]. The low dipole moment and high first hyperpolarizability make it a promising candidate for frequency doubling and optical switching applications. Further, the pyrazole derivates can be used as a photocatalyst and photosensing application.

Docking studies: Using molecular docking experiments, the ligand-protein interaction was used to assess the titled molecule's drug-likeness. In this study, proteins associated with prostate, breast and colon cancers identified by PDB IDs 6XXO, 5W93 and 2HQ6, respectively were selected as targets and retrieved from the Protein Data Bank (PDB) [41-43]. The crystal structures of the target proteins, with respective resolutions of 1.5 Å, 1.7 Å and 2.1 Å, were analyzed using AutoDock 2 for molecular docking with the ligand, while PyMOL animation software [44] was used to visualize the interactions; prior to docking, water molecules were removed, Kollman charges were added to stabilize the proteins and the active sites were predicted using the grid box approach [45].

Docking with 6XXO: In order to fix its orientation in the active site, the ligand forms many hydrogen bonds with LEU-370 and VAL-368 after making a strong interaction with 6XXO. The presence of the pyrazole ring facilitates π–π stacking interactions with key residues, while interactions with ALA-546, LYS-362 and ARG-548 suggest a favourable fit within the binding pocket. The oxygen lone pair of the morpholine moiety enables hydrogen bonding and may also participate in weak polar interactions. Furthermore, the Ramachandran plot (Fig. 9c) confirms the stability of the compound's conformation within the active site.

Docking with 5W93: As shown in Fig. 9e, the ligand forms significant interactions within the active site of 5W93, particularly with residues LEU-759, VAL-766, ALA-774, and THR-763. The morpholine oxygen and pyrazole nitrogen contribute to the ligand's stability by participating in key hydrogen bonding interactions. Although the Ramachandran plot indicates fewer hydrogen bonds compared to 6XXO, it still reflects a well-adapted and stable binding mode.

Docking with 2HQ6: Strong hydrogen bonds are formed between the ligand and residues ASP-108 and ALA-102, while electrostatic interactions with ARG-56 indicate a charge-based attraction that significantly enhances ligand affinity. The dimethylbenzenamine moiety appears to help in ligand retention within the binding pocket by reinforcing hydrophobic inter-

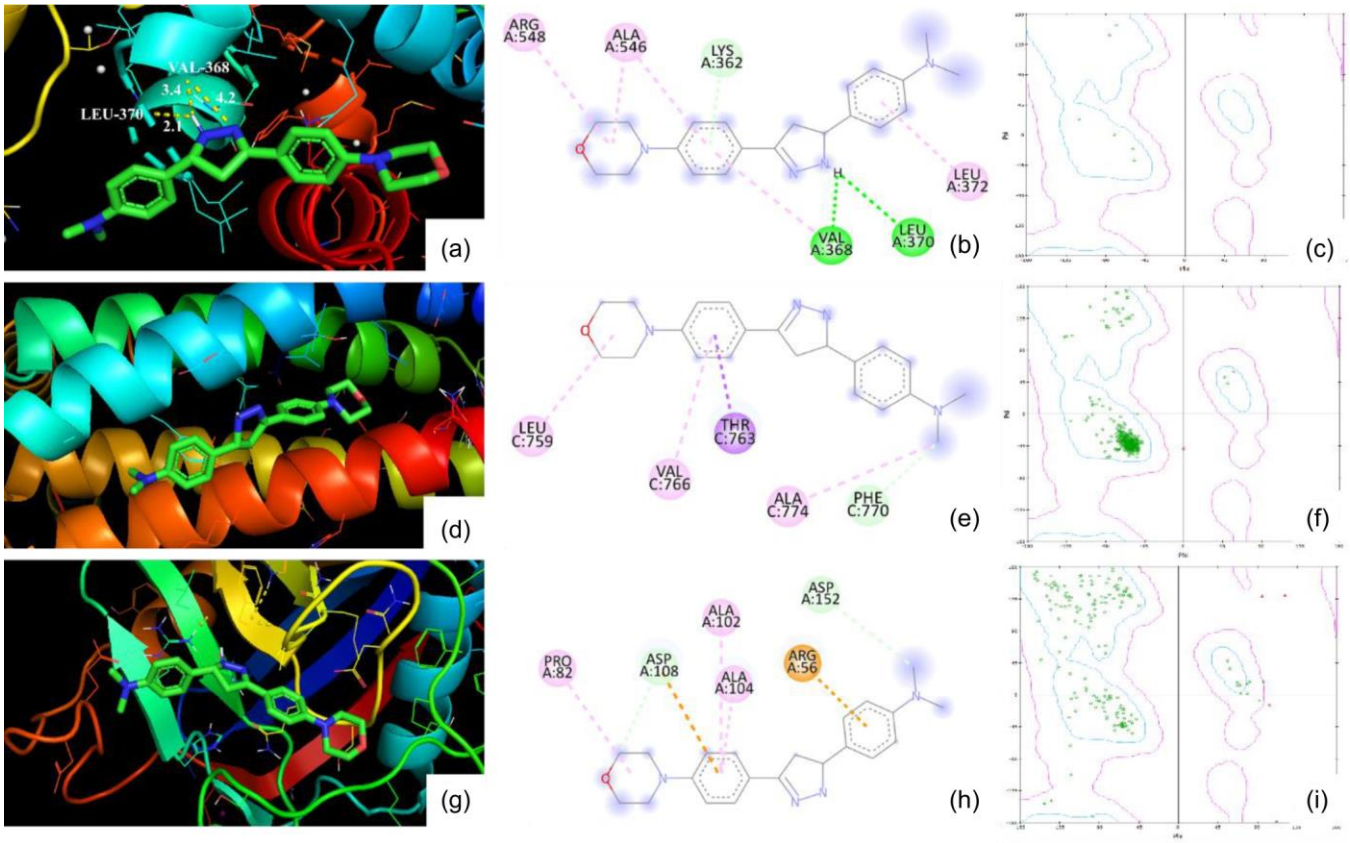

Fig. 9. (a) 3D Docking image with prostate cancer, (b) 2D interaction, (c) Ramachandran plot, (d) 3D docking image with breast cancer, (e) 2D interaction, (f) Ramachandran plot, (g) 3D docking image with colon cancer, (h) 2D interaction and (i) Ramachandran plot

actions with PRO-82 and ALA-104. Molecular docking results suggest that the most favourable binding target for the ligand DMH is 6XXO, followed by 5W93 and 2HQ6. The dimethylbenzenamine group, morpholine oxygen and pyrazole moiety contribute critically to the electrostatic, hydrophobic and hydrogen bonding interactions, respectively. Differences in binding affinity across the proteins can be attributed to variations in the shape of the active sites and the nature of residue interactions. The docking score and interactions details of DMH molecule is shown in Table-4.

ELF and LOL analysis: Fig. 10a illustrates the electron localization function (ELF) of the molecule, providing insight into electron pairing and distribution. High ELF values, represented by red regions, indicate strong electron localization, particularly around the lone pair on the nitrogen atom, highlighting its pronounced non-bonding character. The π-electron delocalization is observed within the aromatic rings, while the oxygen atom in the morpholine ring also exhibits localized electron density. Overall, the ELF analysis confirms that electron localization is concentrated at electronegative sites specifically nitrogen and oxygen atoms, which is consistent with the reactivity and interaction potential of the titled molecule [46].

The localized orbital locator (LOL) analysis was used to evaluate orbital interactions, revealing strong localization in σ-bonds (C–C, C–N and C–O), particularly within the rigid core of the DMH molecule. These regions display moderate localization, indicative of electron-rich centers that may facilitate non-covalent interactions. Elevated LOL values near hydrogen atoms correspond to robust bonding interactions with adjacent atoms, especially within the aniline and pyrazoline moieties. Together, the ELF and LOL analyses suggest that the DMH possesses a well-distributed electronic structure characterized by localized electron density at heteroatoms and bonding regions, alongside moderate delocalization throughout the conjugated framework.

Reduced density gradient (RDG) analysis: The RDG image was generated by the Multiwfn and the VMVD software to predict the type of interaction in the molecule [47]. A strong attractive interaction was observed around the hydrogen bonding detected from the blue region. A weak van der Waals interaction is generally observed in the non-bonded atoms in

TABLE-4
DOCKING SCORE AND INTERACTION DETAILS OF DMH

Protein (PDB ID)	Type of protein	Key interactions	Docking score	Binding strength
6XXO	Prostate cancer	LEU-370, VAL-368, ALA-546, LYS-362, ARG-548	-7.8	Strongest
5W93	Breast cancer	LEU-759, THR-763, PHE-770	-6.8	Moderate
2HQ6	Colon cancer	ASP-108, ALA-102, ARG-56	-6.6	Moderate to weak

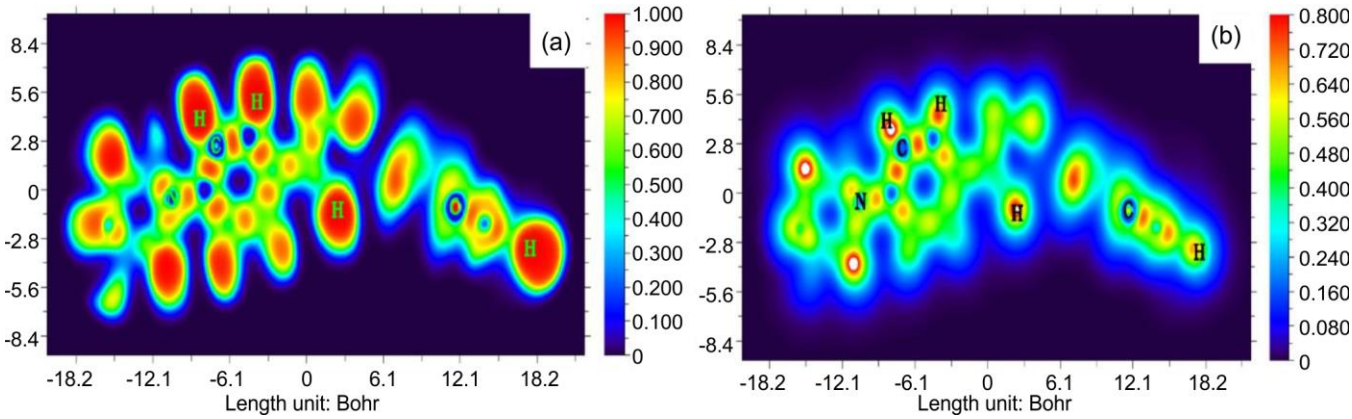

Fig. 10. (a) ELF mapping and (b) LOL mapping of DMH molecule

the rings; in present case, it was observed in the pyrazoline and phenyl groups. From Fig. 11a, the steric repulsion was observed in the red region near the morpholine oxygen. The π-π stacking interaction over the hydrogen bonding and the weak van der Waals forces were confirmed by the scatter plot (Fig. 11b).

ADME: The physico-chemical properties of DMH molecule were predicted from ADME investigations [48]. With a molecular weight of 350.46 g/mol, the chemical formula, $C_{21}H_{26}N_4O$, was also confirmed. The structure revealed that there were four total rotatable bonds and the topological polar surface area (TPSA) was 40.10 Å2 [49]. The drug-likeness of the compound meets Lipinski, Ghose and Muegge criteria and they show intermediate solubility and high GI absorption. Consequently, the molecule has a significant capacity for both oral and central nervous system active medicines and shows favourable pharmacokinetics with high GI absorption. It was discovered that the synthetic accessibility was 3.68, which was more potent than other useful medications (Fig. 12).

Conclusion

In summary, the synthesis and spectral characterization of 4-(4,5-dihydro-3-(4-morpholinophenyl)-1*H*-pyrazol-5-yl)-*N*,*N*-dimethylbenzenamine (DMH) were successfully performed and evaluated using both experimental and quantum chemical methods. Theoretical calculations provided insights into the bond lengths, bond angles, charge transfer mechanisms and electrophilicity, which align well with the experimental findings. The FT-IR analysis confirmed the presence of key functional groups, while NMR spectroscopy validated the structural integrity of the molecule, with chemical shifts closely matching theoretical predictions. UV-Vis analysis demonstrated strong π→π* transitions, with an experimental absorption peak at 300 nm and a theoretical peak at 319 nm, further supporting the electronic properties. HOMO-LUMO analysis revealed a band gap of 4.26 eV, indicating significant molecular stability and moderate reactivity. Furthermore, the molecular docking studies against 6XXO, 5W93 and 2HQ6 confirmed strong binding affinities, suggesting that the ligand exhibits potential inhibitory activity against prostate cancer-related proteins. The interaction analysis highlighted key hydrogen bonding and hydrophobic interactions that reinforce its binding efficiency. These promising results indicate that the synthesized molecule could serve as a biologically active compound with potential anticancer properties. Further, *in vitro* and *in vivo* studies will be necessary to validate its therapeutic potential.

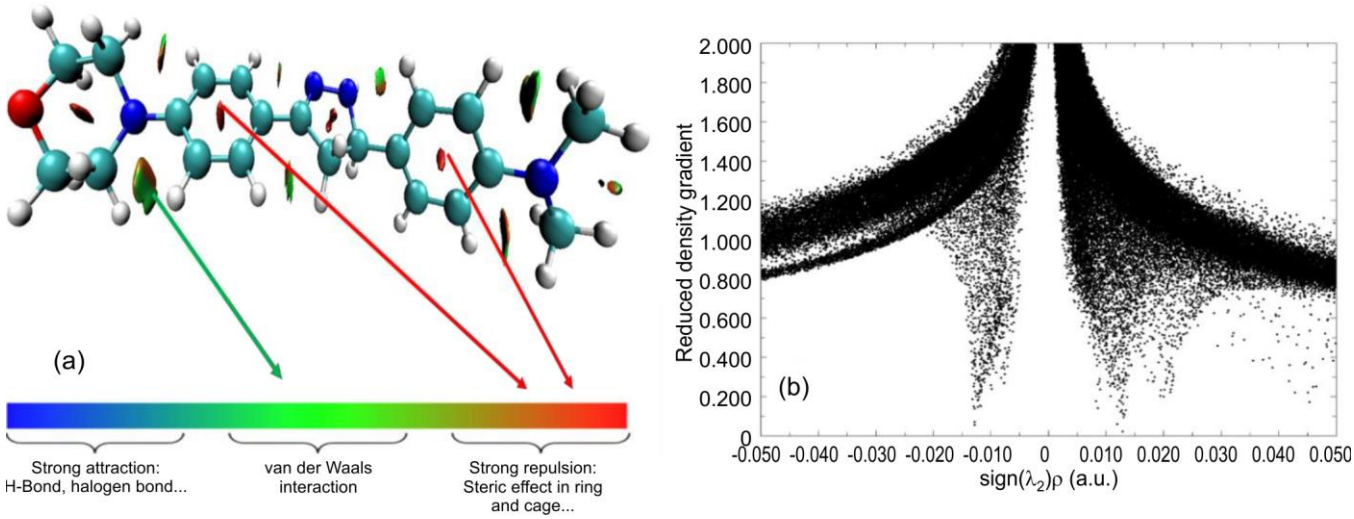

Fig. 11. (a) Non-covalent interaction (NCI) plot and (b) reduced density gradient map of DMH molecule

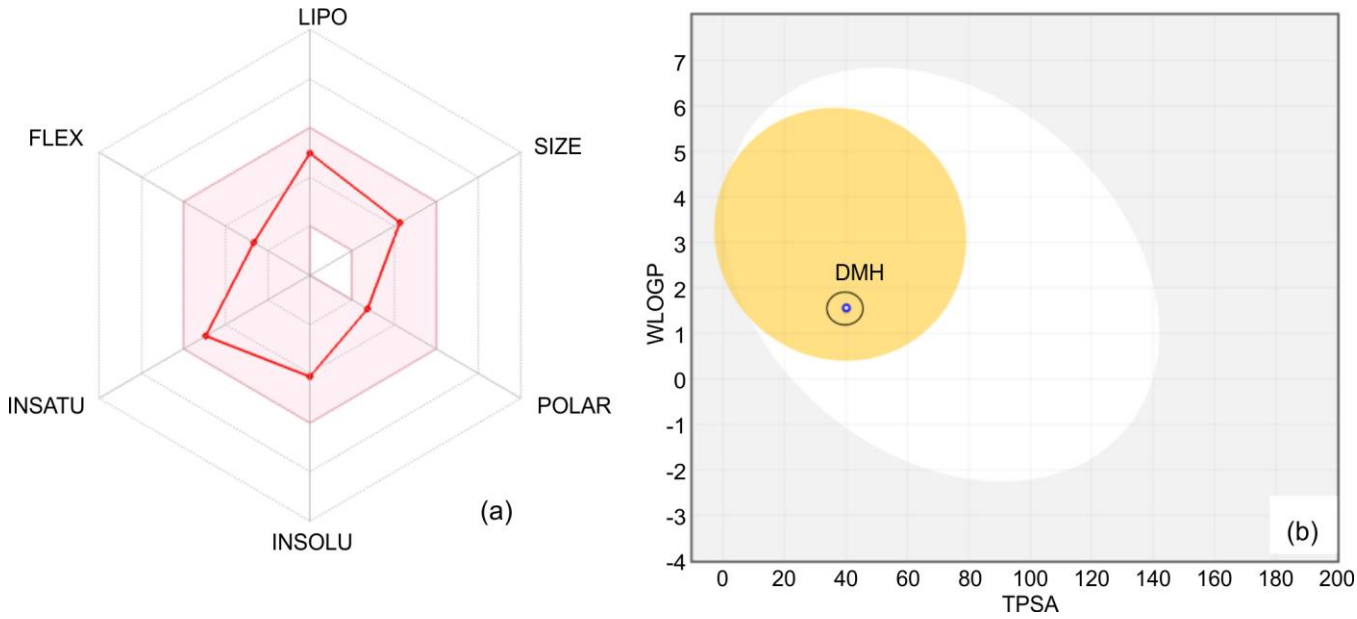

Fig. 12. (a) ADME radar mapping and (b) boiled egg model of DMH molecule

CONFLICT OF INTEREST

The authors declare that there is no conflict of interests regarding the publication of this article.

REFERENCES

1. A.P. Kourounakis, D. Xanthopoulos and A. Tzara, *Med. Res. Rev.*, **40**, 709 (2020); https://doi.org/10.1002/med.21634
2. A. Kumari and R.K. Singh, *Bioorg. Chem*., **96**, 103578 (2020); https://doi.org/10.1016/j.bioorg.2020.103578
3. F. Arshad, M. F. Khan, W. Akhtar, M.M. Alam, L.M. Nainwal, S.K. Kaushik, M. Akhter, S. Parvez, S.M. Hasan and M. Shaquiquzzaman, *Eur. J. Med. Chem.*, **167**, 324 (2019); https://doi.org/10.1016/j.ejmech.2019.02.015
4. K.K. Goel, P. Singhal, E. Sathish, M.A. Babu, S.K. Pandey, Y. Tyagi, R. Kumar, T.G. Singh and S. Puri, *Synlett*, **14** (2024); https://doi.org/10.1055/a-2508-9961
5. G. Mancuso, A. Midiri, E. Gerace and C. Biondo, *Pathogens*, **10**, 1310 (2021); https://doi.org/10.3390/pathogens10101310
6. D. Chiodi and Y. Ishihara, *Eur. J. Med. Chem.*, **273**, 116364 (2024); https://doi.org/10.1016/j.ejmech.2024.116364
7. T.J. Ritchie and S.J.F. Macdonald, *Drug Discov. Today*, **14**, 1011 (2009); https://doi.org/10.1016/j.drudis.2009.07.014
8. E. Lanzarotti, L.A. Defelipe, M.A. Marti and A.G. Turjanski, *J. Cheminform.*, **12**, 30 (2020); https://doi.org/10.1186/s13321-020-00437-4
9. M.F. Khan, M.M. Alam, G. Verma, W. Akhtar, M. Shaquiquzzaman and M. Akhter, *Eur. J. Med. Chem.*, **120**, 170 (2016); https://doi.org/10.1016/j.ejmech.2016.04.077
10 B. Nehra, M. Kumar, V. Chawla and P.A. Chawla, *Futur. J. Pharm. Sci.*, **11**, 75 (2025); https://doi.org/10.1186/s43094-025-00821-7
11. A. Kapri, N. Gupta and S. Nain, *Pharm. Chem. J.*, **58**, 252 (2024); https://doi.org/10.1007/s11094-024-03141-x
12. K. Karrouchi, S. Radi, Y. Ramli, J. Taoufik, Y.N. Mabkhot, F.A. Al-aizari and M. Ansar, *Molecules*, **23**, 134 (2018); https://doi.org/10.3390/molecules23010134
13. G.H. Sayed, M.E. Azab, K.E. Anwer, M.A. Raouf and N.A. Negm, *J. Mol. Liq.*, **252**, 329 (2018); https://doi.org/10.1016/j.molliq.2017.12.156
14. I. Ameziane El Hassani, K. Rouzi, H. Assila, K. Karrouchi and M. Ansar, *Reactions*, **4**, 478 (2023); https://doi.org/10.3390/reactions4030029
15. A.B. Nielsen and A.J. Holder, Gauss View 5.0, User's Reference. GAUSSIAN Inc., Pittsburgh (2009).
16. M.J. Frisch, G.W. Trucks, H.B. Schlegel, G.E. Scuseria, M.A. Robb, J.R. Cheeseman, G. Scalmani, V. Barone, B. Mennucci, G.A. Petersson, H. Nakatsuji, M. Caricato, X. Li, H.P. Hratchian, A.F. Izmaylov, J. Bloino, G. Zheng, J.L. Sonnenberg, M. Hada, M. Ehara, K. Toyota, R. Fukuda, J. Hasegawa, M. Ishida, T. Nakajima, Y. Honda, O. Kitao, H. Nakai, T. Vreven, J.A. Montgomery, Jr., J.E. Peralta, F. Ogliaro, M. Bearpark, J.J. Heyd, E. Brothers, K.N. Kudin, V.N. Staroverov, R. Kobayashi, J. Normand, K. Raghavachari, A. Rendell, J.C. Burant, S.S. Iyengar, J. Tomasi, M. Cossi, N. Rega, J.M. Millam, M. Klene, J.E. Knox, J.B. Cross, V. Bakken, C. Adamo, J. Jaramillo, R. Gomperts, R.E. Stratmann, O. Yazyev, A.J. Austin, R. Cammi, C. Pomelli, J.W. Ochterski, R.L. Martin, K. Morokuma, V.G. Zakrzewski, P. Salvador, J.J. Dannenberg, G.A. Voth, S. Dapprich, A.D. Daniels, O. Farkas, J.B. Foresman, J.V. Ortiz, J. Cioslowski and D.J. Fox, Gaussian 09, Revision A.02, Gaussian, Inc., Wallingford CT (2009).
17. M. Chemek, F.I.H. Rhouma, M. Chemek, Z. Safi, A. Kadi, S. Naili, N. Wazzan and A. Kamel, *J. Mol. Model.*, **30**, 271 (2024); https://doi.org/10.1007/s00894-024-06062-4
18. R. Huey, G.M. Morris and S. Forli, Using AutoDock 4 and AutoDock vina with AutoDockTools: A Tutorial; The Scripps Research Institute Molecular Graphics Laboratory (2012).
19. R.G. Pearson, *Proc. Natl. Acad. Sci. USA*, **83**, 8440 (1986); https://doi.org/10.1073/pnas.83.22.8440
20. A. Dennis Raj, M. Jeeva, M. Shankar, G. Venkatesa Prabhu, M. Vimalan and I. Vetha Potheher, *J. Mol. Struct.*, **1147**, 763 (2017); https://doi.org/10.1016/j.molstruc.2017.06.133
21. N. Rao, Y. Ding, L. Yang, Y. Zhou, Y. Le, L. Yan and L. Liu, *Mol. Cryst. Liq. Cryst.*, **757**, 95 (2023); https://doi.org/10.1080/15421406.2022.2138112
22. M.R. Elmorsy, F.H. Abdelhamed, A. Alqahtani, E. Abdel-Latif, A.A. Abdel-Shafi and M.A. Ismail, *Opt. Mater.*, **151**, 115386 (2024); https://doi.org/10.1016/j.optmat.2024.115386
23. H. Medetalibeyoglu, H. Yüksek and G. Özdemir, *Turk. Comput. Theor. Chem.*, **3**, 76 (2019); https://doi.org/10.33435/tcandtc.469783
24. J. Hafeez, A. Sabir, N. Rasool, U. Hafeez, F. Siddique, M. Bilal, A. Kanwal, G. Ahmad, F. Alqahtani, I. Imran and M. Imran, *Arab. J. Chem.*, **17**, 105889 (2024); https://doi.org/10.1016/j.arabjc.2024.105889

25. H. Yalazan, B. Barut, G. Sarki, B. Ertem, Y. Ünver, A. Özel and H. Kantekin, *J. Coord. Chem.*, **72**, 2409 (2019); https://doi.org/10.1080/00958972.2019.1648795
26. D.R. Thandra, R.R. Bojja and R. Allikayala, *SN Appl. Sci.*, **2**, 1765 (2020); https://doi.org/10.1007/s42452-020-03525-0
27. V. Darugar, M. Vakili, S.F. Tayyari and F.S. Kamounah, *J. Mol. Graph. Model.*, **107**, 107976 (2021); https://doi.org/10.1016/j.jmgm.2021.107976
28. Y. Kaddouri, F. Abrigach, N. Mechbal, Y. Karzazi, M. El Kodadi, A. Aouniti and R. Touzani, *Mater. Today Proc.*, **13**, 956 (2019); https://doi.org/10.1016/j.matpr.2019.04.060
29. S.D. Oladipo, N.O. Obi-Egbedi, M.D. Adeoye, N.D. Ojo and A.A. Badeji, *Scientia Africana*, **22**, 243 (2023); https://doi.org/10.4314/sa.v22i1.21
30. H.N. Hafez, H.-A. Abbas and A.-R. El-Gazzar, *Acta Pharm.*, **58**, 359 (2008); https://doi.org/10.2478/v10007-008-0024-1
31. K. J. Roberson, P. N. Brady, M. M. Sweeney and M. A. Macnaughtan, *J. Vis. Exp.*, **82**, e50875 (2013); https://doi.org/10.3791/50875
32. V.D. Vitnik, Ž.J. Vitnik, N.R. Banjac, N.V. Valentic, G.S. Ušæumlic and I.O. Juranic, *Spectrochim. Acta A Mol. Biomol. Spectrosc.*, **117**, 42 (2014); https://doi.org/10.1016/j.saa.2013.07.099
33. M. Rezaeivala, M. Ahmadi, B. Captain, M. Bayat, M. Saeidirad, S. Sahin-Bölükbasi, B. Yildiz and R.W. Gable, *Inorg. Chim. Acta*, **513**, 119935 (2020); https://doi.org/10.1016/j.ica.2020.119935
34. K. Anbukarasi, S. Xavier, A.H. Hasan, Y.L. Er, J. Jamalis, S. Sebastian and S. Periandy, *Curr. Phys. Chem.*, **13**, 37 (2023); https://doi.org/10.2174/1877946812666220928102954
35. S. Xavier and S. Periandy, *Spectrochim. Acta A Mol. Biomol. Spectrosc.*, **149**, 216 (2015); https://doi.org/10.1016/j.saa.2015.04.055
36. K. Anbukarasi, S. Xavier, J. Jamalis, S. Sebastian, F. Paularokiadoss, S. Periandy and R. Rajkumar, *J. Mol. Struct.*, **1249**, 131580 (2022); https://doi.org/10.1016/j.molstruc.2021.131580
37. S. Sakthivel, T. Alagesan, S. Muthu, C.S. Abraham and E. Geetha, *J. Mol. Struct.*, **1156**, 645 (2018); https://doi.org/10.1016/j.molstruc.2017.12.024
38. T. Sivaranjani, S. Xavier and S. Periandy, *J. Mol. Struct.*, **1083**, 39 (2015); https://doi.org/10.1016/j.molstruc.2014.11.035
39. S. Asokan, S. Sebastian, B. Karthikeyan, S. Xavier, R.G. Raman, S. Silvan, S.S. Margreat and R. Sagayaraj, *Chem. Phys. Impact*, **8**, 100497 (2024); https://doi.org/10.1016/j.chphi.2024.100497
40. H. Hilary, P. Dhamodharan, D. Manimaran, G. Mariappan, R. Aarthi, G. Vijayakumar and D. Rajeswari, *J. Mol. Struct.*, **1320**, 139608 (2025); https://doi.org/10.1016/j.molstruc.2024.139608
41. L. Rosenfeld, A. Sananes, Y. Zur, S. Cohen, K. Dhara, S. Gelkop, E. Ben Zeev, A. Shahar, L. Lobel, B. Akabayov, E. Arbely and N. Papo, *J. Med. Chem.*, **63**, 7601 (2020); https://doi.org/10.1021/acs.jmedchem.0c00418
42. C. Zhang, D.J. Miller, C.D. Guibao, D.M. Donato, S.K. Hanks and J.J. Zheng, *J. Biol. Chem.*, **292**, 18281 (2017); https://doi.org/10.1074/jbc.M117.807271
43. T.L. Davis, J.R. Walker, V. Campagna-Slater, R. Paramanathan, P.J. Finerty, G. Bernstein, F. MacKenzie, W. Tempel, H. Ouyang, W.H. Lee, E.Z. Eisenmesser and S. Dhe-Paganon, *PLoS Biol.*, **8**, e1000439 (2010); https://doi.org/10.1371/journal.pbio.1000439
44. S. Yuan, H.C.S. Chan and Z. Hu, *Wiley Interdiscip. Rev. Comput. Mol. Sci.*, **7**, e1298 (2017); https://doi.org/10.1002/wcms.1298
45. J. Fan, A. Fu and L. Zhang, *Quant. Biol.*, **7**, 83 (2019); https://doi.org/10.1007/s40484-019-0172-y
46. G. Kishore, P. Pritha, S. Xavier, F. Paularokiadoss, D. Bhakiaraj and S. Periandy, *Inorg. Chem. Commun.*, **178**, 11491 (2025); https://doi.org/10.1016/j.inoche.2025.114491
47. A. Innasiraj, B. Anandhi, Y. Gnanadeepam, N. Das, F. Paularokiadoss, A.V. Ilavarasi, C.D. Sheela, D.R. Ampasala and T.C. Jeyakumar, *J. Mol. Struct.*, **1265**, 133450 (2022); https://doi.org/10.1016/j.molstruc.2022.133450
48. A. Daina, O. Michielin and V. Zoete, *Sci. Rep.*, **7**, 42717 (2017); https://doi.org/10.1038/srep42717
49. P. Pritha, G. Kishore, S. Xavier, F. Paularokiadoss, D. Bhakiaraj, G. Bouzid, S. Periandy and S. Ayachi, *Mater. Chem. Phys.*, **326**, 129829 (2024); https://doi.org/10.1016/j.matchemphys.2024.129829